Available online at www.sciencedirect.com
ScienceDirect
Trans. Nonferrous Met. Soc. China 34(2024) 2619−2628
Transactions of Nonferrous Metals Society of China
www.tnmsc.cn

Effect of Mo and ZrO_2 nanoparticles addition on interfacial properties and shear strength of Sn58Bi/Cu solder joint

Amares SINGH[1], Hui Leng CHOO[1], Wei Hong TAN[2], Rajkumar DURAIRAJ[3]

1. School of Engineering, Faculty of Innovation & Technology, Taylor's University, Subang Jaya, 47500, Selangor, Malaysia;
2. Faculty of Mechanical Engineering & Technology, Universiti Malaysia Perlis (UniMAP), Pauh Putra Campus, 02600 Arau, Perlis, Malaysia;
3. Lee Kong Chian Faculty of Engineering and Science, Universiti Tunku Abdul Rahman, Jalan Sungai Long, Bandar Sungai Long, 43000 Kajang, Selangor, Malaysia

Received 3 March 2023; accepted 12 September 2023

Abstract: The influence of Mo and ZrO_2 nanoparticles addition on the interfacial properties and shear strength of Sn58Bi solder joint was investigated. The interfacial microstructures of Sn58Bi/Cu, Sn58Bi + Mo/Cu and Sn58Bi + ZrO_2/Cu solder joints were analysed using a scanning electron microscope (SEM) coupled with energy dispersive X-ray (EDX) and the X-ray diffraction (XRD). Intermetallic compounds (IMCs) of $MoSn_2$ are detected in the Sn58Bi + Mo/Cu solder joint, while SnZr, Zr_5Sn_3, ZrCu and $ZrSn_2$ are detected in Sn58Bi + ZrO_2/Cu solder joint. IMC layers for both composite solders comprise of Cu_6Sn_5 and Cu_3Sn. The SEM images of these layers were used to measure the IMC layer's thickness. The average IMC layer's thickness is 1.4431 μm for Sn58Bi + Mo/Cu and 0.9112 μm for Sn58Bi + ZrO_2/Cu solder joints. Shear strength of the solder joints was investigated via the single shear lap test method. The average maximum load and shear stress of the Sn58Bi + Mo/Cu and Sn58Bi + ZrO_2/Cu solder joints are increased by 33% and 69%, respectively, as compared to those of the Sn58Bi/Cu solder joint. By comparing both composite solder joints, the latter prevails better as adding smaller sized ZrO_2 nanoparticles improves the interfacial properties granting a stronger solder joint.

Key words: lead-free solder; interfacial microstructure; IMC layer thickness; shear strength; dislocation density; ZrO_2 nanoparticles; Mo nanoparticles

1 Introduction

Soldering is the process applied in electronics packaging assembly especially on printed circuit boards (PCBs) to provide interconnection between the board and the electronic components [1,2]. While the growth in the advancement of the soldering technology is eminent, the utilisation of lead solder has still been debated for over some time. The tin (Sn)−lead (Pb) solder serves as the mother solder for the interconnection. The debate over its health threat due to lead contamination calls for its replacement [3]. The ability of the SnPb solder to react with copper (Cu) which is the main element in the PCB board is creditable and some lead-free solders such as SnAgCu, SnAg, and SnBi provide close beneficial influence as the lead solder [4]. While the SnAgCu and SnAg solders compete well with the SnPb solder, the high melting point possessed by these lead-free solders raises alarm concerning the thermal failure during soldering. On

Corresponding author: Amares SINGH, E-mail: amares.singh@taylors.edu.my
DOI: 10.1016/S1003-6326(24)66564-7

the other hand, SnBi possesses low melting point, but investigations on this solder are still in early stages.

Replacing lead with bismuth (Bi) as the alloying element seems promising, with the production of the SnBi solder alloy. This solder is categorized as a low melting point solder alloy, that is beneficial to avoiding high temperature defects to the electronic component during soldering. At eutectic composition (Sn−58wt.%Bi), the solder's melting point is about 139 °C according to the phase diagram [5]. This temperature is 44 °C lower than that of SnPb solder [5,6]. However, the mechanical properties of SnBi solder such as the shear and tensile strength are not akin to those of SnPb solder. The mechanical properties of a solder joint are dependent on the interfacial properties of solder joint. The interface properties of a solder joint relate to the microstructure and the IMC layer that is formed between the solder and substrate. The low melting point of SnBi requires lower reflow soldering compared to that of SnPb, hence making the interconnection between the SnBi and Cu weak, as far as some studies are concerned. Moreover, the content of Bi should be kept preferably at eutectic composition, as higher content will cause the solder joint to be brittle because of the nature of Bi being a brittle metal [3].

Adding nanoparticles seemingly boosted the mechanical properties of solders and has been adopted as the remedy to improve performance of most solders. Reinforcing nanoparticles into high-temperature lead-free solder alloys like SnAgCu [7−9], SnAg [10,11] and SnZn [12,13] shows favourable outcomes. For example, the ultimate tensile strength of nickel oxide (NiO)/ zirconia ZrO nanoparticles added SnAgCu solder joint was recorded as 38.4 MPa compared to 27.9 MPa recorded for the plain SnAgCu solder joint [14]. The increase was attributed to the existence of NiO/ZrO nanoparticles that acted as the load bearing to the strain and refined the Ag_3Sn and Cu_6Sn_5 IMCs at the interface. The fracture morphology was of dimple type ductile fracture. Similarly, in another study, dimple fracture morphology was observed on the fracture surface of Sn0.5Ag0.7Cu/Cu joint added with 1% alumina (Al_2O_3) nanoparticles [8]. The study also reported that the shear force of the Al_2O_3-added solder joint was higher consistently with ageing at different temperatures compared to that of the plain solder. Research by XING et al [15] also showed an increase in the hardness and tensile strength of the Al_2O_3-added Sn9Zn solder. On another note, ZrO_2 nanoparticles additions showed improvement in the shear load of the Sn9Zn/Cu solder joint for all different reflow cycles compared to that of the plain Sn9Zn/Cu joint [16]. The molybdenum (Mo) nanoparticles were also added to some solder systems, and one of them was reported in the study done by YANG et al [17]. The research stated that there was a need for greater critical stress for dislocations to pass through the second-phase Mo particles and consequently made it harder for the dislocation to bypass the particles. Elsewhere, both Cu_6Sn_5 and Cu_3Sn IMC layer thickness of the Mo-added SnAgCu solder joint was thinner by almost half as compared to that of the plain solder joint [18]. Such reports suggest that the additions of nanoparticles could improve a solder's properties. Still, most of such studies were focused on high-temperature solder alloys with limited research on low-temperature solder alloys such as SnBi. The application of low-temperature solder in the electronic industry is beneficial as lower reflow soldering temperature could be used. This would protect other electronic components from high-temperature shock or damage and avoid the warpage of the solder joint.

In the present study, Mo and ZrO_2 nanoparticles were mixed into the eutectic SnBi solder alloy and soldered to the Cu substrate. The microstructural compound and the IMC layer at the interface of the SnBi and Cu joint were analysed. As these interfacial properties influence the mechanical properties of a solder joint, this research also focuses on establishing the relationship between the interfacial properties and shear strength of the Mo and ZrO_2 nanoparticles added SnBi solder joints.

2 Experimental

2.1 Solder alloy preparation

Three sets of solder alloys were prepared, one of them is the reference solder, the eutectic Sn58Bi, and the other two are the Mo and ZrO_2 nanoparticles reinforced Sn58Bi solder. The total mass of reference solder alloy was set as 20 g. The Sn58Bi solder alloy was prepared by melting the Sn

and Bi elements together in a heat treatment furnace at a constant temperature of 600 °C with a holding time of 1.5 h to ensure proper melting and homogenous mixing. Later, the solder alloy was let to cool until 200 °C in the furnace itself to avoid any contamination and oxidation. The molten solder of Sn58Bi was taken out and heated in a hot plate and then poured onto a ceramics plate to solidify. After that, the solidified solder alloy was compressed to a thickness of 1 mm and punched to billets of 5 mm in diameter for soldering purposes. The Mo and ZrO_2 nanoparticles were weighted to be 0.6 g. The Mo and ZrO_2 nanoparticles were mixed into the Sn58Bi solder alloy at 300 °C and the stirring process was done concurrently. The temperature was chosen as 300 °C with the intention to mix the nanoparticles as discrete particles. In addition, at 300 °C, both the Sn and Bi will be in the liquid state, and hence during the solidification, the effect of the nanoparticle's additions to the Sn58Bi solder would be consistent from the liquid to solid phase. Both nanoparticles have an average size of less than 50 nm, where the average size of Mo nanoparticles is 48.5 nm and that of the ZrO_2 nanoparticles is 29 nm. The SEM images of these nanoparticles are shown in Fig. 1. Before casting into billet forms, the molten solder of the Sn58Bi + Mo and Sn58Bi + ZrO_2 composite solders were poured to an alumina crucible for re-melting accompanied with mechanical stirring on the molten solder. This process was done using a hot plate. Table 1 gives the mass composition of the solder.

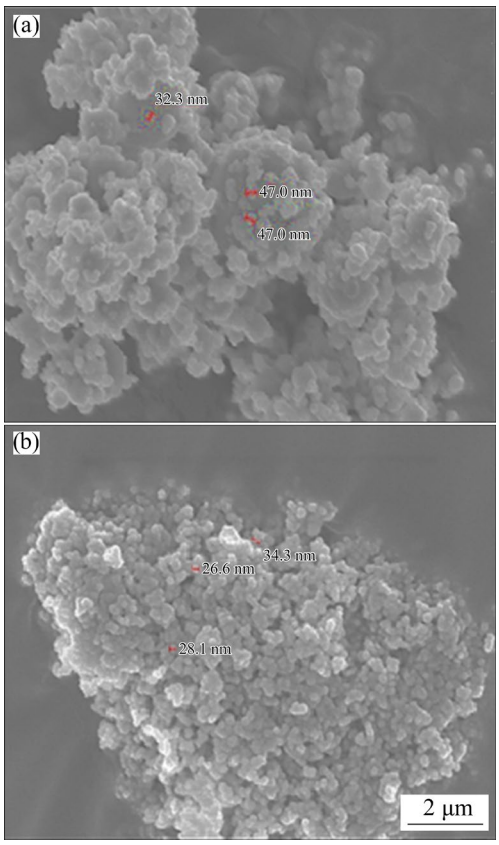

Fig. 1 SEM images of Mo (a) and ZrO_2 (b) nanoparticles

Table 1 Mass compositions of solders

Solder	Mass composition/g			
	Sn	Bi	Mo	ZrO_2
Sn58Bi	8.4	11.6	−	−
Sn58Bi + Mo	8.4	11.6	0.6	−
Sn58Bi + ZrO_2	8.4	11.6	−	0.6

2.2 Soldering process

The soldering process was conducted by employing the dimension used in single shear lap joint method in accordance with the ASTM D1002. Cu substrate was cut to a dimension of 40 mm × 10 mm × 1 mm with a soldering area of 5 mm × 10 mm. Zinc chloride flux was applied on the soldering area of the Cu substrate to prevent the oxidation. The solder billets were placed on the solder area between two Cu substrates and these substrates were fixed to avoid misplacing of the solder. The schematic drawing and real experimental setup of the shear lap joints are shown in Figs. 2(a, b). The fixed shear lap joints were then placed in a heat furnace and the furnace was heated to 230 °C and this temperature was held for 1 min to allow the solder to melt on the substrate. The solder joints were let to solidify inside the furnace to avoid oxidation and contamination. The solidified solder joints are now referred to as reflowed solder joints of Sn58Bi/Cu, Sn58Bi + Mo/Cu and Sn58Bi + ZrO_2/Cu.

2.3 Interfacial characterization and mechanical testing setup

The reflowed solder joints were cut and cold mounted using epoxy resin. The epoxy mounted solder joints were ground using fine SiC papers and polished on the 0.05 μm polishing pad with alumina polish liquid applied to it. The interfacial microstructure and layer of the as-reflowed Sn58Bi,

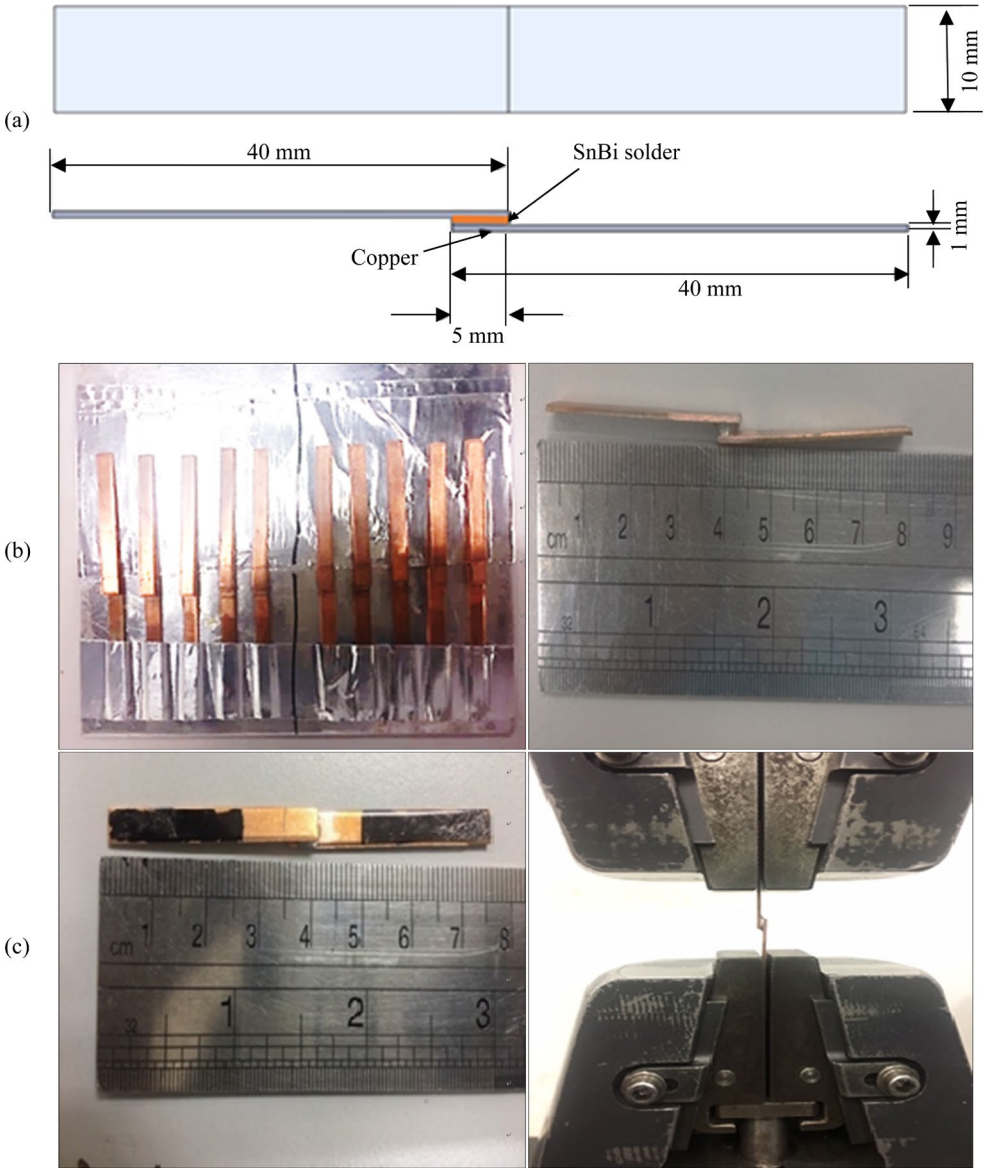

Fig. 2 Schematic drawing of single shear lap solder joint (a); actual sample of single shear lap solder joints (b); grip area of solder joint and actual shear testing setup (c)

Sn58Bi + Mo and Sn58Bi + ZrO_2 were examined using scanning electron microscope (SEM S3400N HITACHI) coupled with energy dispersive X-ray (EDX) and X-ray diffraction (XRD 6000 SHIMADZU). The thickness of the IMC layer at the solder joint was measured using the built-in software in the SEM device. Once the SEM images of the solder joints are captured, the IMC layers were detected first using the EDX and then the XRD analyses. The thickness of these layers is then measured by drawing 10 random vertical red lines from the top of the IMC layer (solder side) to the bottom of the layer (copper side). These lines show the measured thickness and a total of ten measurements are taken to find the average thickness. The shear test was performed using the universal tensile machine (Instron 5582Q4970) at a crosshead speed of 1.3 mm/min. The maximum load (kN) and maximum shear strength (MPa) at break were averaged based on five test samples. The setup of the shear test aligned to the ASTM D1002 standard. The experimental setups for the shear test are shown in Figs. 2(b, c).

3 Results and discussion

3.1 Microstructures of solder joints

The SEM images accompanied by the EDX analyses on the microstructures at the solder joints are shown in Fig. 3. The XRD patterns for SnBi,

Sn58Bi + Mo and Sn58Bi + ZrO_2 composite solder are shown in Fig. 4. The raw results of the XRD results confirming the other phases/compounds are tabulated in Supporting Materials (SM) (Tables S1−S3). The microstructure of the Sn58Bi solder on the solder side consists of a typical alternated lamellar structure of β-Sn (dark phases) and Bi (white phases). Similarly, this lamellar structure is found in the Sn58Bi + Mo and Sn58Bi + ZrO_2 composite solders with the presence of Mo and ZrO_2 nanoparticles. Not much difference in the lamellar structure is observed on the solder side of the Mo- and ZrO_2-added solder compared to that of the reference solder. The nanoparticles are not observed in the image, but their presence is confirmed by the EDX and XRD analyses (red box area in Fig. 3). There are no chunks/agglomeration of the nanoparticles observed from the high-magnification SEM images. Therefore, the nanoparticles are predicted to be dispersed discretely.

Irregular uneven IMC layer is observed for Mo- and ZrO_2-added solder joints at the interface. Again, the existence of Mo and ZrO_2 is confirmed from the EDX and XRD analyses. XRD analyses reveal that the microstructure for all three solder's formulations has common elements and compounds of Bi, Sn, Cu, CuSn, Cu_6Sn_5, with the Cu_6Sn_5 as the

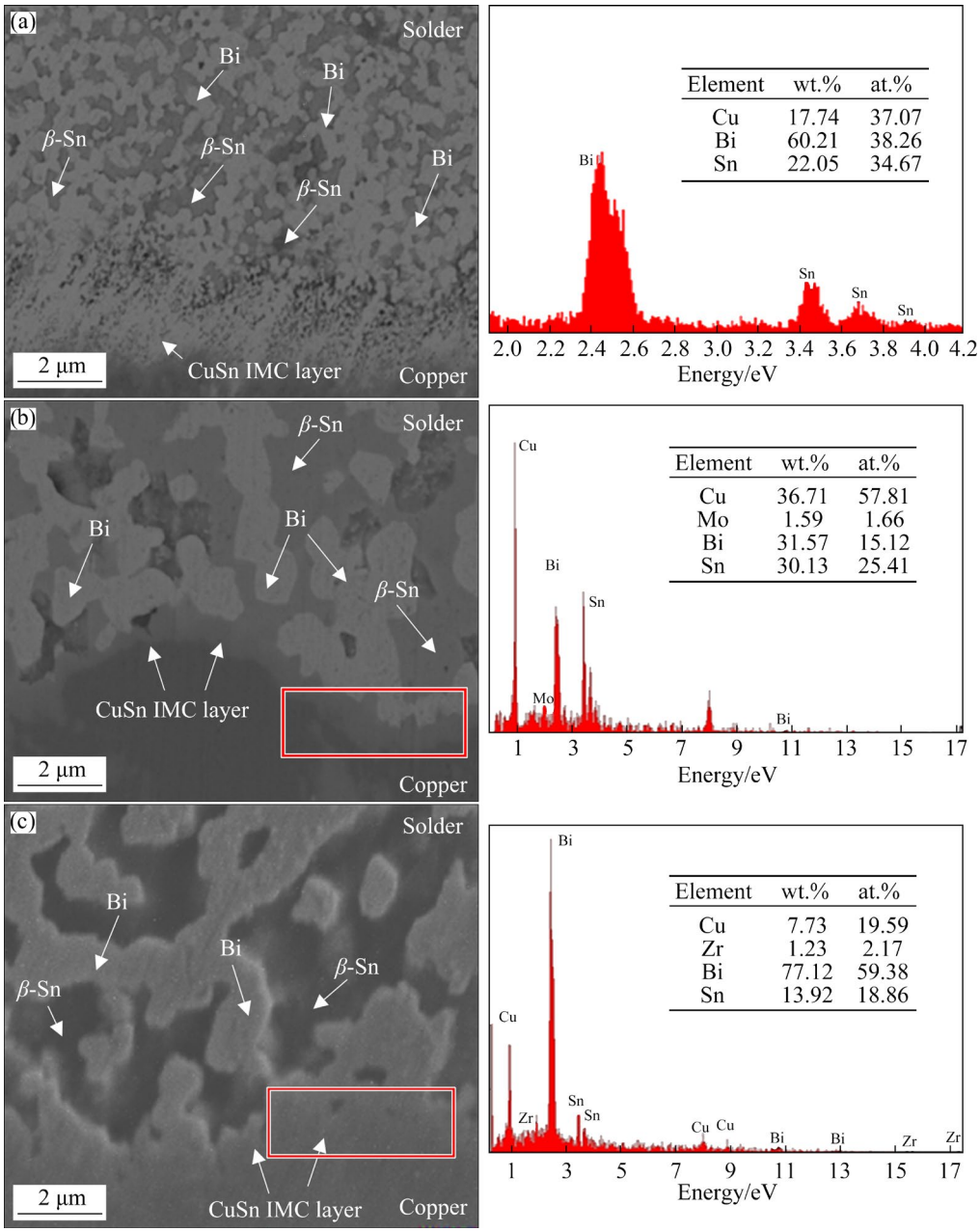

Fig. 3 IMC layer and EDX results of Sn58Bi/Cu (a), Sn58Bi + Mo/Cu (b) and Sn58Bi + ZrO_2/Cu (c) solder joints

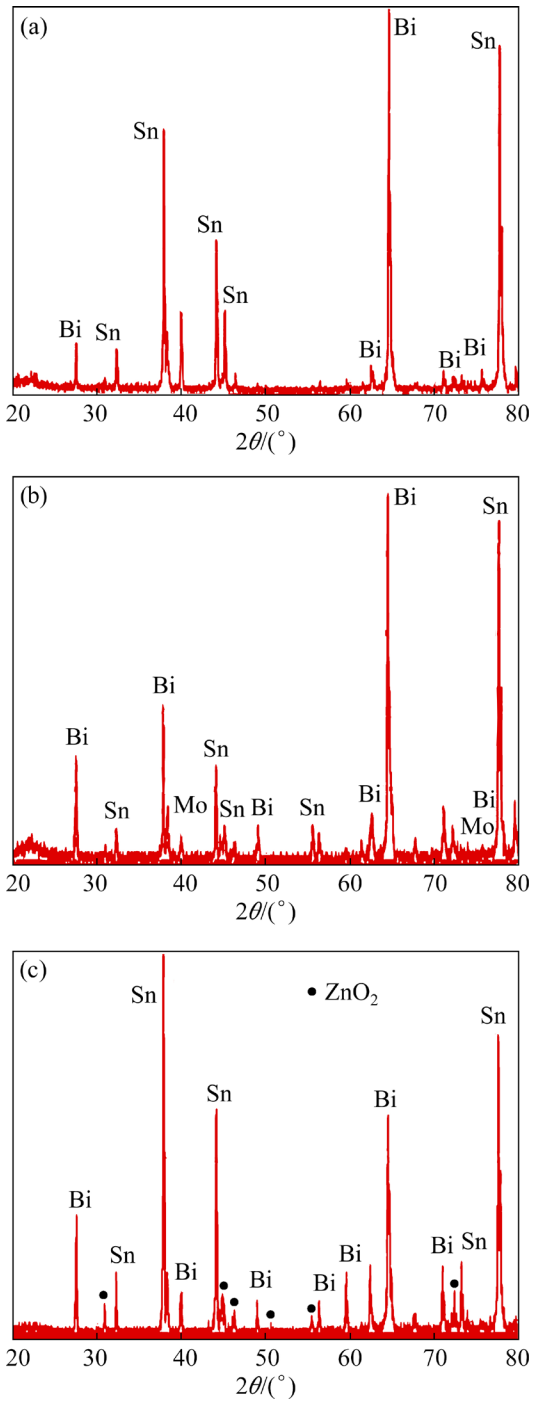

Fig. 4 XRD patterns of Sn58Bi (a), Sn58Bi + Mo (b) and Sn58Bi + ZrO_2 (c) solders

dominant IMC. Other detected compounds are also given in Tables S1−S3 in SM. The Bi does not react with Cu or Sn to form any IMC, while the reactions of Cu towards Sn are more noticeable. The reaction between Cu and Sn forming Cu_6Sn_5 is shown in Eq. (1). Cu_3Sn IMC is formed from the reaction of Cu_6Sn_5 with Cu as shown in Eq. (2). AN and QIN [19] and YI et al [20] observed similar IMCs as a reaction between Sn and Cu. The phase diagram of SnBi also states that these IMCs will be formed at temperatures below 350 °C [21].

$$6Cu+5Sn=Cu_6Sn_5 \quad (1)$$

$$Cu_6Sn_5+9Cu=5Cu_3Sn \quad (2)$$

The IMCs of $MoSn_2$ are also detected through the XRD analysis at the Sn58Bi + Mo solder. It is found that these IMCs assist the formation of the $Cu_{10}Sn_3$ layer as the Sn reacts with Mo to form $MoSn_2$, allowing more Cu to react with Cu_6Sn_5. EDX and XRD results reveal that the discrete Mo nanoparticles are only found on the top side of the IMC layer with less distributions at the interfacial layer, suggesting Mo at the interface mostly has reacted with Sn. In contrast, the ZrO_2 nanoparticles are detected as discrete oxide particles themselves (based on XRD) between the solder and substrate for the Sn58Bi + ZrO_2/Cu solder joint. Moreover, for this composite solder, the interface consists of IMCs like SnO, SnZr, Zr_5Sn_3, ZrCu and $ZrSn_2$. The presence of ZrO_2 allows the Zr to react with Cu and Sn to form these IMCs due to the high reactivity of Zr towards Sn and Cu. The Bi is not detected as it is found to react with O from the ZrO_2 to form the BiO_2 IMCs. The existence of O also allows it to react with Sn and Zr to produce other IMCs like SnO and Zr_3O_1. Crucially, the influence of Zr in reacting with other elements reduces the production of Cu_6Sn_5 and Cu_3Sn IMC layer.

3.2 IMC layer thickness of solder joints

Average IMC layer thicknesses for all solder joints are shown in Fig. 5. The IMC layer's thicknesses are indicated as the red vertical lines in the SEM images in Fig. 6. The average IMC layer's thicknesses of Sn58Bi/Cu, Sn58Bi + Mo/Cu and Sn58Bi + ZrO_2/Cu solder joints are 2.8431, 1.4431 and 0.9112 μm, respectively. The thickness of the IMC layer decreases for both the Mo- and ZrO_2-added solder joints, proving that the presence of these particles assists in the reduction of the IMC layer thickness.

As most of the Mo element reacts with Sn to from $MoSn_2$, there are very few discrete Mo nanoparticles existing at the interfacial layer of CuSn. Therefore, there is no restriction to the diffusion path between Cu and Sn to produce IMC layers of Cu_6Sn_5 and Cu_3Sn, $Cu_{10}Sn_3$. Clearly, the IMC layer's thickness of the Sn58Bi + ZrO_2/Cu

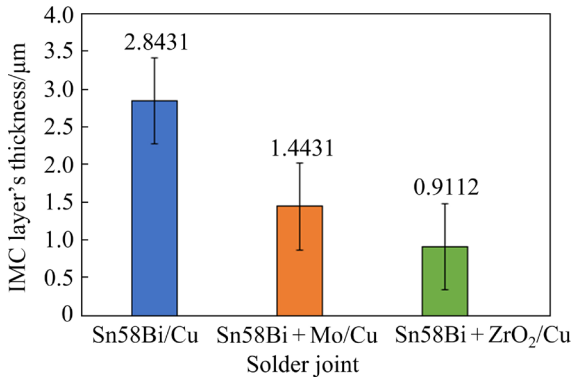

Fig. 5 IMC layer's thickness of Sn58Bi/Cu, Sn58Bi + Mo/Cu and Sn58Bi + ZrO_2/Cu solder joints

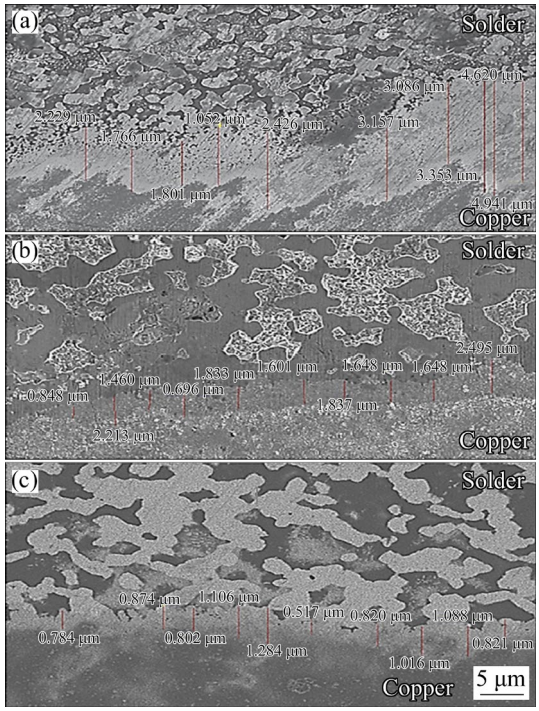

Fig. 6 SEM images of IMC layer's thickness of Sn58Bi/Cu (a), Sn58Bi + Mo/Cu (b) and Sn58Bi + ZrO_2/Cu (c) solder joints

solder joint is less than that of Sn58Bi/Cu and Sn58Bi + Mo/Cu solder joints. The reason for this is most of the ZrO_2 nanoparticles are found to exist as discrete oxide particles and assist in restricting the formation of a thicker IMC layer. As surface active elements, ZrO_2 nanoparticles gather at the interfacial site and block the diffusion movement of Sn from solder and Cu from the substrate, hence hindering the growth of the CuSn IMC layer. The blocking phenomenon is illustrated in Fig. 7. Additionally, other IMCs such as SnZr, Zr_5Sn_3, ZrCu and $ZrSn_2$ further restrict the growth of the CuSn IMC layer. The formation of only Cu_6Sn_5 and Cu_3Sn IMC layers prove that the ZrO_2 nanoparticles and other IMCs in the Sn58Bi + ZrO_2/Cu solder joint restrict the thickening of the IMC layer. Also, the $Cu_{10}Sn_3$ layer is not seen in this solder joint interface. WU et al [8] observed similar retardation in the growth of Cu_3Sn IMC layer with the presence of Al_2O_3 nanoparticles in the SnAgCu/Cu solder joint. Evidently, the IMC layer and its thickness contribute to the strength of solder joints. This explanation was likewise apparent in the studies done by KANLAYASIRI and MOOKAM [22] and CHEN et al [23].

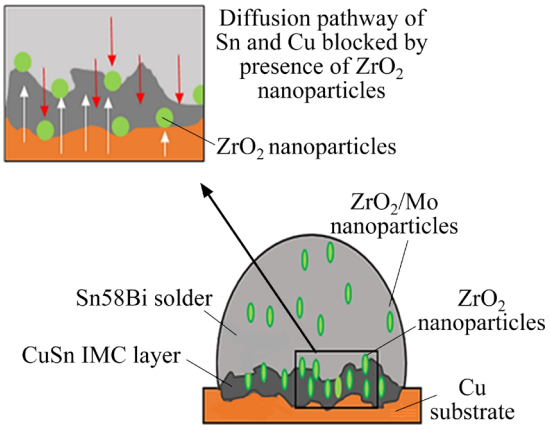

Fig. 7 Blocking of diffusion process by nanoparticles

3.3 Shear strength of solder joints

The shear strength of the solder joints was analysed based on the results of average maximum load and average shear stress. The results are shown in Fig. 8. The average maximum loads for the Sn58Bi/Cu, Sn58Bi + Mo/Cu and Sn58Bi + ZrO_2/Cu solder joints are 514.5, 688.5 and 871.2 N, respectively. The average shear stresses for Sn58Bi/Cu, Sn58Bi + Mo/Cu and Sn58Bi + ZrO_2/Cu solder joints are 104.667, 137.721 and 174.259 MPa, respectively. These trends show that the additions of Mo and ZrO_2 nanoparticles increase the shear strength of the joint, with the ZrO_2 additions having a better result.

The effect of the IMC layer on the shear strength was well explained by HU et al [24,25], presenting the importance of analysing the IMC layer and shear strength. The shear strength results in this research are consistent with the results of the interfacial layer and IMC layer's thickness. Thin IMC layers for the Mo- and ZrO_2-added composite solder help in providing a stronger joint between the solder and Cu substrates, reflecting to higher

average maximum load and average shear stress. A recent study by CHEN et al [23] reported a similar result of a thinner Cu_6Sn_5 IMC layer with the presence of boron carbide (B_4C) nanoparticles contributing to high shear strength. Likewise, the additions of 0.1% Ni-CNT reduced the average IMC layer's thickness of the SnAgCu/Cu which reflected higher shear strength [26]. Thick IMC layers are known to be more prone towards crack initiation and propagation as found for the SnBi/Cu solder joint.

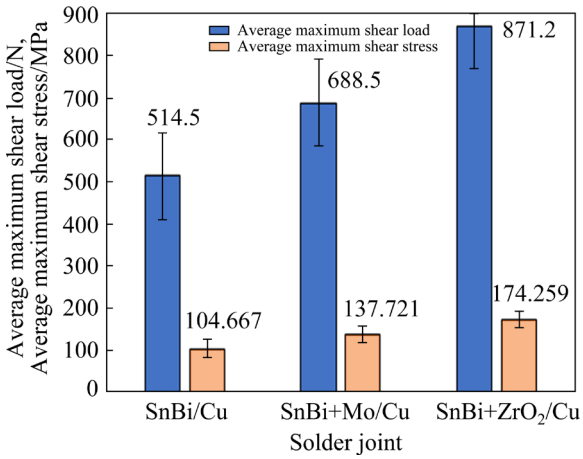

Fig. 8 Average maximum shear load and shear stress of Sn58Bi/Cu, Sn58Bi + Mo/Cu and Sn58Bi + ZrO_2/Cu solder joints

The presence of $MoSn_2$ IMCs at the interfacial site of the Sn58Bi + Mo composite solder joint and SnZr, Zr_5Sn_3, ZrCu and $ZrSn_2$ IMCs at the interfacial site of the Sn58Bi + ZrO_2/Cu composite solder joint provides additional strengthening impact on the solder joint. These IMCs are not part of the IMC layer but exist as additional sole compounds at the interfacial layer and are believed to provide precipitation strengthening effect to the joint. These IMCs are not visible from the SEM images in Figs. 3 and 5 but are detected by the XRD analyses (listed in SM) conducted at these interfaces. The presence of these IMCs creates more dislocation sites and increases the dislocation density at the joint, which concurrently increases the load needed to penetrate or pass through the dislocations. This is in agreement with the studies conducted by KANLAYASIRI and MOOKAM [22] and SINGH et al [27].

The presence of ZrO_2 as discrete particles at the interfacial site of Sn58Bi + ZrO_2/Cu composite solder interface further improves the strength of the solder joint. As discrete and surface-active elements, ZrO_2 nanoparticles are likely to distribute themselves at the interfacial layer and contribute to the strength of solder joints by the theory of second-phase dispersion strengthening. These second-phase fine ZrO_2 nanoparticles restrict the dislocation needed to bypass them and increase the dislocation distortion energy. This phenomenon also resists the movement of the load, promoting the diffusion strengthening. The second-phase dispersion strengthening is also described as the Orowan strengthening effect. MA and WU [28], BI et al [29] and ZHANG et al [30] also reported the improvement in the shear strength due to the strengthening of the IMC layer after adding nanoparticles, which corresponds to the present study. An illustration of the Orowan effect by ZrO_2 nanoparticles is shown in Fig. 9.

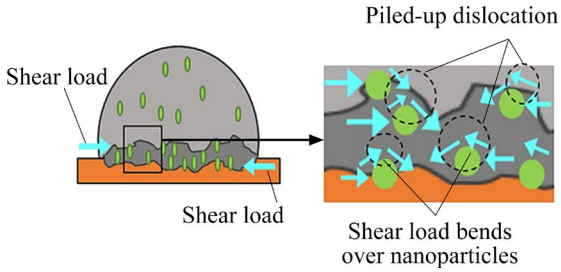

Fig. 9 Shear load looping over ZrO_2 nanoparticles

4 Conclusions

The addition of Mo and ZrO_2 nanoparticles to Sn58Bi solder results in the formation of new intermetallic compounds at the solder/Cu substrate interface. The nanoparticles are observed as discrete particles and their presence suppresses the growth of Cu_6Sn_5 and Cu_3Sn intermetallic layers. This, in turn, leads to a thinner intermetallic layer and enhances shear strength in the Sn58Bi + Mo/Cu and Sn58Bi + ZrO_2/Cu composite solder joints compared to the Sn58Bi/Cu joint. Notably, the Sn58Bi + ZrO_2/Cu composite solder joint exhibits the highest shear strength, likely attributed to the Orowan strengthening effect provided by the discrete ZrO_2 nanoparticles within the IMC layer.

CRediT authorship contribution statement

Amares SINGH: Methodology, Formal analysis, Investigation, Data curation, Writing − Original draft, Results analyses; **Hui Leng CHOO:** Resources,

Writing − Review & editing; **Wei Hong TAN:** Data curation, Formal analysis; **Rajkumar DURAIRAJ:** Resources, Writing − Review & editing, Supervision.

Declaration of competing interest

The authors declare that they have no known competing financial interests or personal relationships that could have appeared to influence the work reported in this paper.

Supporting Materials

Supporting Materials in this paper can be found at: http://tnmsc.csu.edu.cn/download/16-p2619-2023-0255-Supporting_Materials.pdf.

References

[1] LI M L, ZHANG L, JIANG N, ZHANG L, ZHONG S J. Materials modification of the lead-free solders incorporated with micro/nano-sized particles: A review [J]. Materials & Design, 2021, 197: 10924.

[2] ARRIOLA E R, UBANDO A T, GONZAGA J A, LEE C C. Wafer-level chip-scale package lead-free solder fatigue: A critical review [J]. Engineering Failure Analysis, 2023, 144: 1−21.

[3] ISMAIL N, ATIQAH A, JALAR A, ABU B M, RAHIM R A A, ISMAIL A G, HAMZAH A, KENG L K. A systematic literature review: The effects of surface roughness on the wettability and formation of intermetallic compound layers in lead-free solder joints [J]. Journal of Manufacturing Processes, 2022, 83: 68−85.

[4] KUMAR N, MAURYA A. Development of lead free solder for electronic components based on thermal analysis [J]. Materials Today: Proceedings, 2022, 62: 2163−2167.

[5] REN G, WILDING I J, COLLINS M N. Alloying influences on low melt temperature SnZn and SnBi solder alloys for electronic interconnections [J]. Journal of Alloys and Compounds, 2016, 665: 251−260.

[6] MA Y, LI X Z, YANG L Z, ZHOU W, WANG M X, ZHU W B, WU P. Effects of graphene nanosheets addition on microstructure and mechanical properties of SnBi solder alloys during solid-state aging [J]. Materials Science and Engineering A, 2017, 696: 437−444.

[7] GU X, BAI H L, CHEN D D, ZHAO L Y, YI J H, LIU X, YAN J K. The influences of reactive nanoparticles alloying on grain boundary and melting properties about Sn3.0Ag0.5Cu solder [J]. Intermetallics, 2021, 138: 107346.

[8] WU J, HUANG G Q, XUE S B, XUE P, XU Y. Thermal reliabilities of Sn−0.5Ag−0.7Cu−0.1Al_2O_3/Cu solder joint [J]. Transactions of Nonferrous Metals Society of China. 2022, 32: 3312−3320.

[9] HAN Y D, YANG J H, XU L Y, JING H Y, ZHAO L. Effect of transient current bonding on interfacial reaction in Ag-coated graphene Sn−Ag−Cu composite solder joints [J]. Transactions of Nonferrous Metals Society of China, 2021, 31: 2454−2467.

[10] KO Y K, KWON S H, LEE Y K, KIM J K, LEE C W, YOO S. Fabrication and interfacial reaction of carbon nanotube-embedded Sn−3.5Ag solder balls for ball grid arrays [J]. Journal of Alloys and Compounds, 2014, 583: 155−161.

[11] GUO B F, KUNWAR A, ZHAO N, CHEN J, WANG Y P, MA H T. Effect of Ag_3Sn nanoparticles and temperature on Cu_6Sn_5 IMC growth in Sn−*x*Ag/Cu solder joints [J]. Materials Research Bulletin, 2018, 99: 239−248.

[12] GANCARZ T, BOBROWSKI P, JANUZS P, SYLWIA P. Thermal and mechanical properties of lead-free SnZn−*x*Na casting alloys, and interfacial chemistry on Cu substrates during the soldering process [J]. Journal of Alloys and Compounds, 2016, 679: 442−453.

[13] MIN D. Ultrasonic semi-solid soldering 6061 aluminum alloys joint with Sn−9Zn solder reinforced with nano/nano+ micron Al_2O_3 particles [J]. Ultrasonics Sonochemistry, 2019, 52: 150−156.

[14] HUO F P, JIN Z, HAN D L, LI J H, ZHANG K K, NISHIKAWA H. Novel interface regulation of Sn1.0Ag0.5Cu composite solders reinforced with modified ZrO_2: Microstructure and mechanical properties [J]. Journal of Materials Science & Technology, 2022, 125: 157−170.

[15] XING W Q, YU X Y, LI H, MA L, ZUO W, DONG P, WANG W X, DING M. Microstructure and mechanical properties of Sn−9Zn−*x*Al_2O_3 nanoparticles (*x*= 0−1) lead-free solder alloy: First-principles calculation and experimental research [J]. Materials Science and Engineering A, 2016, 678: 252−259.

[16] SHEN J, CHAN Y C. Effects of ZrO_2 nanoparticles on the mechanical properties of Sn−Zn solder joints on Au/Ni/Cu pads [J]. Journal of Alloys and Compounds, 2009, 477: 552−559.

[17] YANG L M, MA S R, MU G W. Improvements of microstructure and hardness of lead-free solders doped with Mo nanoparticles [J]. Materials Letters, 2021, 304: 130654.

[18] YANG L M, QUAN S Y, LIU C, SHI G M. Aging resistance of the Sn−Ag−Cu solder joints doped with Mo nanoparticles [J]. Materials Letters, 2019, 253: 191−194.

[19] AN T, QIN F. Intergranular cracking simulation of the intermetallic compound layer in solder joints [J]. Computational Materials Science, 2013, 79: 1−14.

[20] YI X, ZHANG R H, HU X W. Study on the microstructure and mechanical property of Cu-foam modified Sn3.0Ag0.5Cu solder joints by ultrasonic-assisted soldering [J]. Journal of Manufacturing Processes, 2021, 64: 508−517.

[21] CHANTARAMANEE S, SUNGKHAPHAITOON P. Influence of bismuth on microstructure, thermal properties, mechanical performance, and interfacial behavior of SAC305−*x*Bi/Cu solder joints [J]. Transactions of Nonferrous Metals Society of China, 2021, 31: 1397−1410.

[22] KANLAYASIRI K, MOOKAM N. Influence of Cu content on microstructure, grain orientation and mechanical properties of Sn−*x*Cu lead-free solders [J]. Transactions of Nonferrous Metals Society of China, 2022, 32: 1226−1241.

[23] CHEN C, ZHANG L, WANG X, LU X, GAO L L, ZHAO M, GUO Y H. Mechanical properties and microstructure evolution of Cu/Sn58Bi/Cu solder joint reinforced by B_4C nanoparticles [J]. Journal of Materials Research and

Technology, 2023, 23: 1225−1238.
[24] HU X W, XU T, KEER L M, LI Y L, JIANG X X. Microstructure evolution and shear fracture behavior of aged Sn3Ag0.5Cu/Cu solder joints [J]. Materials Science and Engineering A, 2016, 673: 167−177.
[25] HU X X, XU T, KEER L M, LI Y L, JIANG X X. Shear strength and fracture behavior of reflowed Sn3.0Ag0.5Cu/Cu solder joints under various strain rates [J]. Journal of Alloys and Compounds, 2017, 690: 720−729.
[26] WANG H Z, HU X W, JIANG X X. Effects of Ni modified MWCNTs on the microstructural evolution and shear strength of Sn−3.0Ag−0.5Cu composite solder joints [J]. Materials Characterization, 2020, 163: 110287.
[27] SINGH A, DURAIRAJ R, KUAN S H. Experimental study on the melting temperature, microstructural and improved mechanical properties of Sn58Bi/Cu solder alloy reinforced with 1%, 2% and 3% zirconia (ZrO_2) nanoparticles [J]. Archives of Metallurgy and Materials, 2021, 66(2): 407−418.
[28] MA D L, WU P. Effects of Zn addition on mechanical properties of eutectic Sn−58Bi solder during liquid-state aging [J]. Transactions of Nonferrous Metals Society of China, 2015, 25: 1225−1233.
[29] BI X Y, HU X W, LI Q L. Effect of Co addition into Ni film on shear strength of solder/Ni/Cu system: Experimental and theoretical investigations [J]. Materials Science and Engineering A, 2020, 788: 139589.
[30] ZHANG Z, HU X W, JIANG X X, LI Y L. Influences of mono-Ni(P) and dual-Cu/Ni(P) plating on the interfacial microstructure evolution of solder joints [J]. Metallurgical and Materials Transactions A, 2018, 50: 480−492.

添加 Mo 和 ZrO_2 纳米颗粒对 Sn58Bi/Cu 焊接接头界面性能和剪切强度的影响

Amares SINGH[1], Hui Leng CHOO[1], Wei Hong TAN[2], Rajkumar DURAIRAJ[3]

1. School of Engineering, Faculty of Innovation & Technology, Taylor's University, Subang Jaya, 47500, Selangor, Malaysia;
2. Faculty of Mechanical Engineering & Technology, Universiti Malaysia Perlis (UniMAP), Pauh Putra Campus, 02600 Arau, Perlis, Malaysia;
3. Lee Kong Chian Faculty of Engineering and Science, Universiti Tunku Abdul Rahman, Jalan Sungai Long, Bandar Sungai Long, 43000 Kajang, Selangor, Malaysia

摘　要：研究添加 Mo 和 ZrO_2 纳米颗粒对 Sn58Bi 焊接接头界面性能和剪切强度的影响。利用扫描电子显微镜(SEM)、X 射线能谱仪(EDX)和 X 射线衍射仪(XRD)分析 Sn58Bi/Cu、Sn58Bi + Mo/Cu 和 Sn58Bi + ZrO_2/Cu 的界面显微组织。在 Sn58Bi + Mo/Cu 中检测到了金属间化合物(IMCs)$MoSn_2$，在 Sn58Bi + ZrO_2/Cu 中检测到了 SnZr、Zr_5Sn_3、ZrCu 和 $ZrSn_2$。两种复合材料焊料的 IMC 层均由 Cu_6Sn_5 和 Cu_3Sn 组成。通过 SEM 图测量 IMC 层的厚度，结果表明，Sn58Bi + Mo/Cu 和 Sn58Bi + ZrO_2/Cu 的 IMC 层平均厚度分别为 1.4431 μm 和 0.9112 μm。通过单搭接剪切测试法研究焊接接头的剪切强度。与 Sn58Bi/Cu 焊接接头相比，Sn58Bi + Mo/Cu 和 Sn58Bi + ZrO_2/Cu 焊接接头的平均最大载荷和剪切应力分别提高了 33%和 69%。两种复合材料焊接接头相比，后者表现更佳，这是由于添加尺寸较小的 ZrO_2 纳米颗粒改善了焊接接头的界面性能，从而提高了其强度。

关键词：无铅焊料；界面显微组织；金属间化合物层厚度；剪切强度；位错密度；ZrO_2 纳米颗粒；Mo 纳米颗粒

(Edited by Bing YANG)